

Time Series Analysis of Global Temperature Distributions: Identifying and Estimating Persistent Features in Temperature Anomalies*

Yoosoon Chang[†], Robert K. Kaufmann,[‡] Chang Sik Kim[§],
J. Isaac Miller[¶], Joon Y. Park^{||}, Sungkeun Park^{**}

Abstract

We analyze a time series of global temperature anomaly distributions to identify and estimate persistent features in climate change. Temperature densities from globally distributed data during the 1850 to 2012 period are treated as a time series of functional observations that change over time. We employ a formal test for the existence of functional unit roots in the time series of these densities. Further, we develop a new test to distinguish functional unit roots from functional deterministic trends or explosive behavior. We find some persistent features in global temperature anomalies, which are attributed in particular to significant portions of mean and variance changes in their cross-sectional distributions. We detect persistence that characterizes a unit root process, but none of the persistence appears to be deterministic or explosive.

This Version: July 25, 2016

JEL Classification: C14, C23, C33, Q54

Key words and phrases: climate change, temperature distribution, global temperature trends, functional unit roots

*The authors are grateful for useful comments from William A. “Buz” Brock, Jim Stock, participants of the 2016 SNDE Symposium, 2015 INET-Cambridge Workshop, 2014 NBER-NSF Conference, and 2014 SETA, and seminar attendees at University of Carlos III, University of Pompeu Fabra, CEMFI, Carleton University, Korea University, Seoul National University, Vienna University of Economics and Business, CORE, USC, University of Notre Dame, Hitotsubashi University, Maastricht University, and University of Missouri. This work was supported by the National Research Foundation of Korea Grant funded by the Korean government (NRF-2014S1A5B8060964). The usual caveat applies.

[†]Department of Economics, Indiana University

[‡]Department of Earth and Environment, Boston University

[§]Department of Economics, Sungkyunkwan University

[¶]Corresponding author. Address correspondence to J. Isaac Miller, Department of Economics, University of Missouri, 118 Professional Building, Columbia, MO 65211, or to millerjisaac@missouri.edu.

^{||}Department of Economics, Indiana University and Sungkyunkwan University

^{**}Korea Institute for Industrial Economics and Trade

1 Introduction

Though they may seem like statistical minutiae, the questions of whether the time series for temperature and radiative forcing contain a stochastic and/or deterministic trends are important. The properties of these time series are critical for the detection and attribution of climate change. Identifying the presence of such trends is a key step in testing hypotheses about the physical principles that are postulated to drive climate change, how climate change will affect the likelihood of weather extremes, and the recently postulated notion of a hiatus in warming. Moreover, the time series properties affect the statistical techniques that are appropriate for analyzing the observational record and simulation results. For example, Monte Carlo simulations indicate that statistical models designed to detect a deterministic trend will find a deterministic trend in about 85% of realizations that contain only a stochastic trend (Hendry and Juselius, 2000).

First principles imply that the time series for radiative forcing and temperature contain a stochastic trend. There is no physical mechanism that can cause radiative forcing or temperature to rise or fall by the same amount year after year. Consistent with this notion, climate models are initialized to a steady-state, not a constant rate of change. Hence, the statistical identification of and distinction between stochastic and deterministic trends lies at the heart of efforts to test the physical mechanisms hypothesized to drive climate change.

Similarly, first principles suggest that the highly persistent movements in the radiative forcing of greenhouse gases and sulfur emissions are caused by (a) the long-lived nature of capital stock, which emits these gases, and (b) the relatively long residence time of these gases, which allows the atmosphere to integrate emissions into concentrations (Kaufmann *et al.*, 2013). The transmission of this persistence in radiative forcing to temperature is consistent with the basic physics that are embodied in climate models. A zero dimension energy balance model can be rewritten in the form of an error correction model typically used to analyze relations among time series with common stochastic trends (Kaufmann *et al.*, 2013).

Given the underlying importance of the time series properties, a significant literature focuses on detecting a trend in temperature and distinguishing a linear trend from lower-order unit root-type persistence (i.e. a stochastic trend). To date, the evidence is mixed. Many studies generate results that are consistent with the presence of a stochastic trend (Gordon, 1991; Woodward and Gray, 1993, 1995; Gordon *et al.* 1996; Kärner, 1996). Conversely, many other studies generate results that are consistent with the presence of a deterministic trend with possibly highly persistent noise (Bloomfield, 1992; Bloomfield and Nychka, 1992; Baillie and Chung, 2002; Fomby and Vogelsang, 2002).

Although Bloomfield (1992) tests for a linear trend, he emphasizes the importance of using a model-based nonlinear deterministic component. Accordingly, the notion of a deterministic trend also includes nonlinearities in the form of a quadratic trend (Woodward and Gray, 1995; Zheng and Basher, 1999), an exponential trend (Zheng *et al.*, 1997), and breaks in an otherwise linear trend (Zheng *et al.*, 1997; Zheng and Basher, 1999; Gay-Garcia *et al.*, 2009; Estrada *et al.*, 2010, 2013; Estrada and Perron, 2012, 2014; McKittrick and Vogelsang, 2014). Nonlinearity also is investigated by estimating a general deterministic trend nonparametrically (Gao and Hawthorne, 2006). Their results suggest that the estimated trend contains high degrees of nonlinearity and variability, which can be approximated by a stochastic trend.

Beyond tests on individual time series, the presence of stochastic trends is examined by testing whether temperature cointegrates with radiative forcing. If these variables cointegrate, the shared stochastic trend would be consistent with the hypothesis that economic activity and atmospheric lifetimes impart a stochastic trend to radiative forcing and this trend is communicated to temperature. Many studies find evidence of this cointegration (Kaufmann and Stern, 2002; Kaufmann *et al.*, 2006a, 2011, Mills, 2009; Dergiades *et al.*, 2016).

These results are disputed by those who argue that cointegration is a statistical artifact of a broken deterministic trend (Gay *et al.*, 2009). In reply, Kaufmann *et al.* (2010) argue that the appearance of a broken deterministic temperature trend is inherited from the forcing variables, which may suggest a break in the 1980's due to legislation limiting acid deposition. The addition of weather variability makes the stochastic trend difficult to detect (Kaufmann *et al.*, 2013). Estrada *et al.* (2013) use simulated temperatures to eliminate weather variability, and they find a break.

Examination of cross-sectional means along the lines of the studies mentioned above is useful, but it ignores the global distributions of temperatures (Ballester *et al.*, 2010; Donat and Alexander, 2012). Moreover, Brock *et al.* (2013) underscore the importance of spatial heterogeneity – temperature anomalies increase with latitude (Hansen *et al.*, 2010). For example, Zheng and Basher (1999) argue that stronger variability in high latitudes of the Northern Hemisphere make it difficult to detect a deterministic trend in local temperature anomalies. The effects of heterogeneity can be better understood by considering higher-order moments of the spatial distribution of the anomalies.

Given the potential importance of nonstationary trends, it is now possible to evaluate the stationarity or nonstationarity of cross-sectional distributions, such as distributions of global temperature anomalies (Bosq, 2000; Park and Qian, 2012; Chang *et al.*, 2016). Using these tools, analysts can evaluate the persistence in the mean and the higher-order moments

of the global distributions of temperature anomalies.

Building on these capabilities, we extend the work of Chang *et al.* (2016) to distinguish between persistence that is induced by unit root-type nonstationarity (a stochastic trend) from that induced by a deterministic trend or an explosive root in distributions of temperature anomalies (global, Northern Hemisphere and Southern Hemisphere) during the instrumental record (1850-2012). Our tests allow for much richer temporal dynamics than recent spatio-temporal climate models, which assume temporal stationarity (e.g., Castruccio and Stein, 2013), allow for nonstationarity only in the forms of “modest” dependence (Castruccio *et al.*, 2014), or seasonal variations (Leeds *et al.*, 2015). However, we do not model any spatial covariances; therefore, our assumptions about the spatial dimension are more restrictive than the sophisticated and possibly nonstationary spatial covariances in the spatial models of Jun and Stein (2008) *inter alia*, and the recent spatio-temporal model of Castruccio and Stein (2013).

Our results identify substantial nonstationarity in the first four moments of the distributions – primarily in the mean (i.e., global warming) and in the (decreasing) global variance. We postulate that a natural experiment, in which anthropogenic forcings differ between hemispheres, generate hemispheric differences in the persistence of the mean, the number of nonstationary coordinate processes, and the skewness. Together, these results suggest that stochastic trends in radiative forcing can be used as fingerprints to attribute changes in temperature to human activity. Conversely, none of the nonstationarity that we detect is more persistent than that of a stochastic trend. Such evidence casts doubt on the type of (deterministic) trend, which would imply that changes in the moments – in particular, an increasing mean – are inevitable. As such, these results are inconsistent with the notion that (a) temperature can be modeled using a deterministic trend, (b) the so-called hiatus in warming represents a physical change in the mechanisms that affect global temperature, or (c) warming is being accelerated by a so-called runaway greenhouse effect.

Our results and the methods used to obtain them are described in the following three sections. In Section 2, we introduce the global temperature anomaly data, and we discuss the time series framework for analyzing state distributions and testing procedures for non-stationarity of those distributions. We discuss step-by-step implementation of the tests and present our empirical results in Section 3, and we discuss these results in the context of the extant literature in Section 4. Section 5 concludes.

2 Data and Methodology

First, we first present the data set of global temperature anomalies used in our analysis. We then review the basic time series framework and methodology used by Chang *et al.* (2016) to test for nonstationarity of state distributions. Because this procedure may be new to many readers, our discussion is self-contained but necessarily abbreviated, and interested readers are referred to that paper for additional technical details.

Although the methodology and theory of our analysis are largely based on Chang *et al.* (2016), our procedure contains a novel aspect. While they consider a test for nonstationarity against only a stationary left-hand-sided alternative, we extend their test to an explosive or deterministically trending right-hand-sided alternative. The extension is critical to discern persistence that characterizes a unit root process from much stronger persistence in temperature anomalies.

2.1 Global Temperature Distributions

We employ the HadCRUT3 data set, which is well-known to climate researchers and is described in detail by Brohan *et al.* (2006). The data set combines marine temperature data compiled by the Met Office Hadley Centre with land temperature data compiled by the Climatic Research Unit of the University of East Anglia. These monthly measurements extend from 1850 to 2012 and aim to cover as much of the globe as possible.

The HadCRUT3 data report temperature anomalies in degrees Celsius from the monthly average over the period 1961-90. Specifically, deviations are calculated for each land station (110 - 4,098 stations per month throughout the sample), and then the deviations are averaged across all stations in a given grid box that is 5° latitude by 5° longitude. For marine data, the measurements are taken from ships or buoys (1,495 - 1,648,815 marine observations per month throughout the sample), and the anomaly is calculated based on the monthly average over 1961-90 for each grid box. The interested reader is referred to Brohan *et al.* (2006) for a very detailed discussion of data construction and known limitations, such as warming effects from urbanization and technological changes in measuring temperature over the previous century and a half.

The maximum number of temperature anomaly observations in each month is given by 2,592, the product of 36 increments of 5° latitude and 72 increments of 5° longitude. We create an annual distribution of temperature anomaly observations from the monthly HadCRUT3 data, providing a maximum number of $2,592 \times 12 = 31,104$ annual observations. Figure 1 shows annual time series of the number of non-empty box-months for the globe and for each hemisphere. Observations per year generally increase from about 5,000 at the

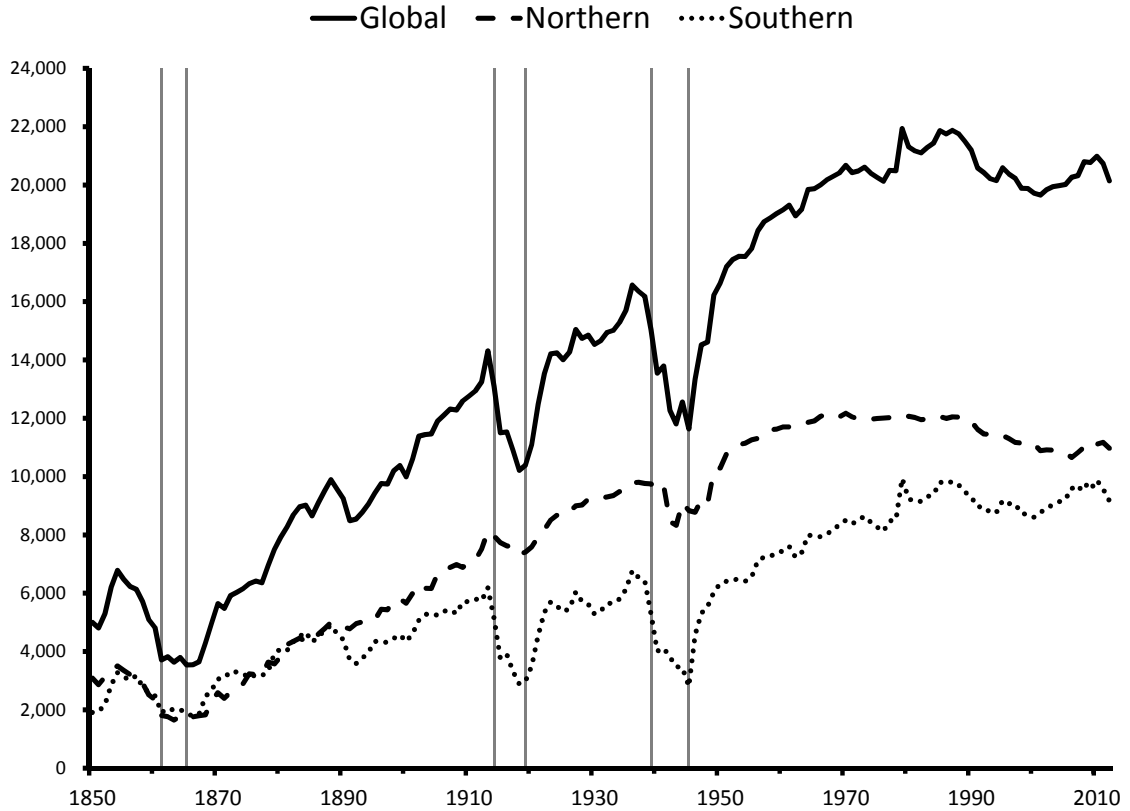


Figure 1: Number of Annual Temperature Observations. Observations for the globe, NH, and SH, based on 5° by 5° grid boxes. Total possible annual observations for the globe is $36 \times 72 \times 12 = 31,104$ ($36 \times 5^\circ$ along each meridian, $72 \times 5^\circ$ around the Equator, 12 months per year) and 15,552 for each hemisphere. American Civil War (1861-65), World War I (1914-19), and World War II (1939-45) indicated.

beginning of the sample to about 22,000 in the mid-1990's, leveling out at about 21,000 by the end of the sample. There are three obvious dips, which correspond roughly with the American Civil War (1861-65), World War I (1914-19), and World War II (1939-45).

Hemispheric means often are analyzed separately in studies on climate change, because more land in the Northern Hemisphere (NH) translates into more error from station and other types of biases, but less land in the Southern Hemisphere (SH) translates into more small-sample and coverage errors from fewer non-missing grid box observations. Global means are estimated by averaging the hemispheric means. (Brohan *et al.*, 2006.)

Working with densities requires a more complicated averaging strategy. We obtain the temperature distributions from the monthly temperature anomaly data pooled over each year in the NH and SH. We estimate the densities of temperature anomalies for the

NH and SH separately. Then, for each year and at each temperature, we average the estimated NH and SH density functions to obtain an estimate of the global density function at that temperature. The global density is described by the density function over a compact subset of temperatures. Each hemisphere receives an equal weight to avoid giving too much weight to the NH, where there are more non-empty grid boxes. We omit approximately 1% extreme outliers and make the supports of these densities compact.¹ Specifically, we set the supports $[-4.98, 4.76]$, $[-6.06, 5.68]$, and $[-3.32, 3.075]$ for the global, NH, and SH distributions, respectively. We utilize the typical nonparametric density estimator with the Epanechnikov kernel and Silverman bandwidth to estimate the densities.

The estimated densities are regarded as the data that we subsequently analyze. We expect that estimation errors in the temperature anomaly densities have a negligible effect on our analysis, because the number of cross-sectional observations each year is very large relative to the number of years. The estimation errors decrease with the cross-sectional dimension, but they are expected to accumulate as the time dimension increases. Therefore, we treat the densities as being observable in our subsequent discussions.

Let $f_t(s)$ denote the value of a temperature anomaly density at time t and ordinate s (temperature anomaly), for $t = 1, \dots, T$ and $s \in \mathbb{R}$. We define the *temporal mean* of a time series (f_t) of temperature anomaly densities as $\bar{f}_T(s) = T^{-1} \sum_{t=1}^T f_t(s)$ for $s \in \mathbb{R}$, and the *cross-sectional mean* as $\mu_t = \int s f_t(s) ds$ for $t = 1, \dots, T$.² The top left panel of each of Figures 2-4 shows the annual temperature anomaly densities $(f_t(s))$. Specifically, Figure 2 shows the global densities, Figure 3 shows those for the NH, and Figure 4 shows those for the SH. The temporally demeaned temperature anomaly densities $-(w_t(s))$ in our subsequent notation – are shown in the top right panels of the respective figures. We interpret the latter as deviations from the average probability of observing a temperature anomaly over the sample time span. For example, in all of the figures, the probability of observing a $+1^\circ\text{C}$ temperature anomaly appears to be below average in 1850 but above average in 2012, whereas the probability of observing -1°C appears to be the reverse. Clearly, these are neither constant over time, as a flat graph would imply, nor do they appear to be generated by random noise.

The remaining panels of Figures 2-4 show the time paths of the estimated *cross-sectional moments* of the distributions (f_t) . Specifically, the means (middle left panels), variances

¹The compact supports avoid the well-known empty bin problem in nonparametric density estimation. We note that the HadCRUT3 data already omits extreme temperature anomalies in its construction (Brohan *et al.*, 2006). We do not believe that our omission should substantially affect our qualitative results, since our aim is to describe global rather than local anomalies.

²We may, of course, compute the cross-sectional mean as a Riemann sum using a fine enough partition over the support of the given density function.

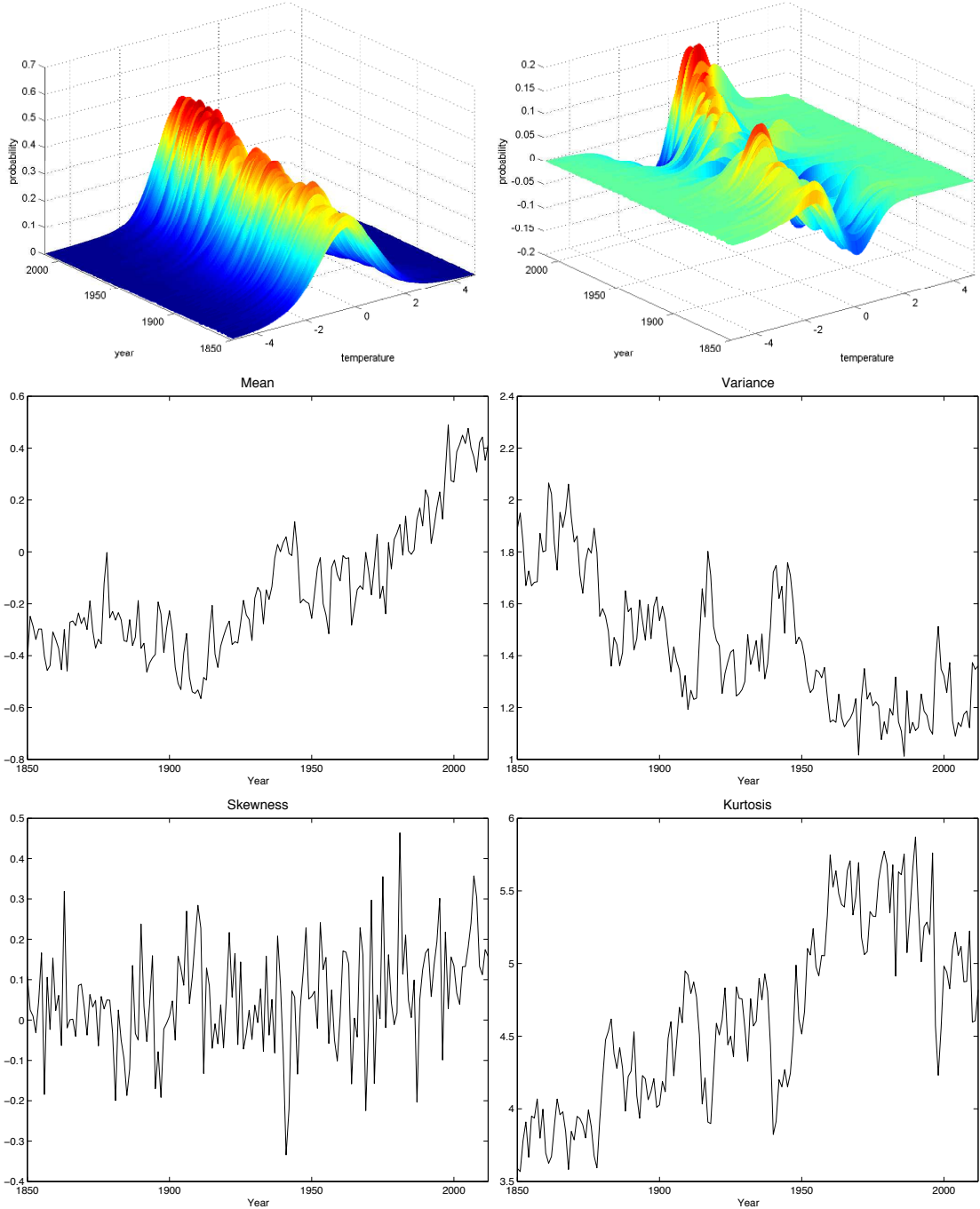


Figure 2: Global Temperature Anomaly Densities and Moments. Annual temperature anomalies measured on a 5° by 5° grid box. Undemeaned densities (top left panel) and temporally demeaned global densities (top right panel). Sample mean (middle left panel), variance (middle right panel), skewness (bottom left panel), and kurtosis (bottom right panel) of annual anomalies over time.

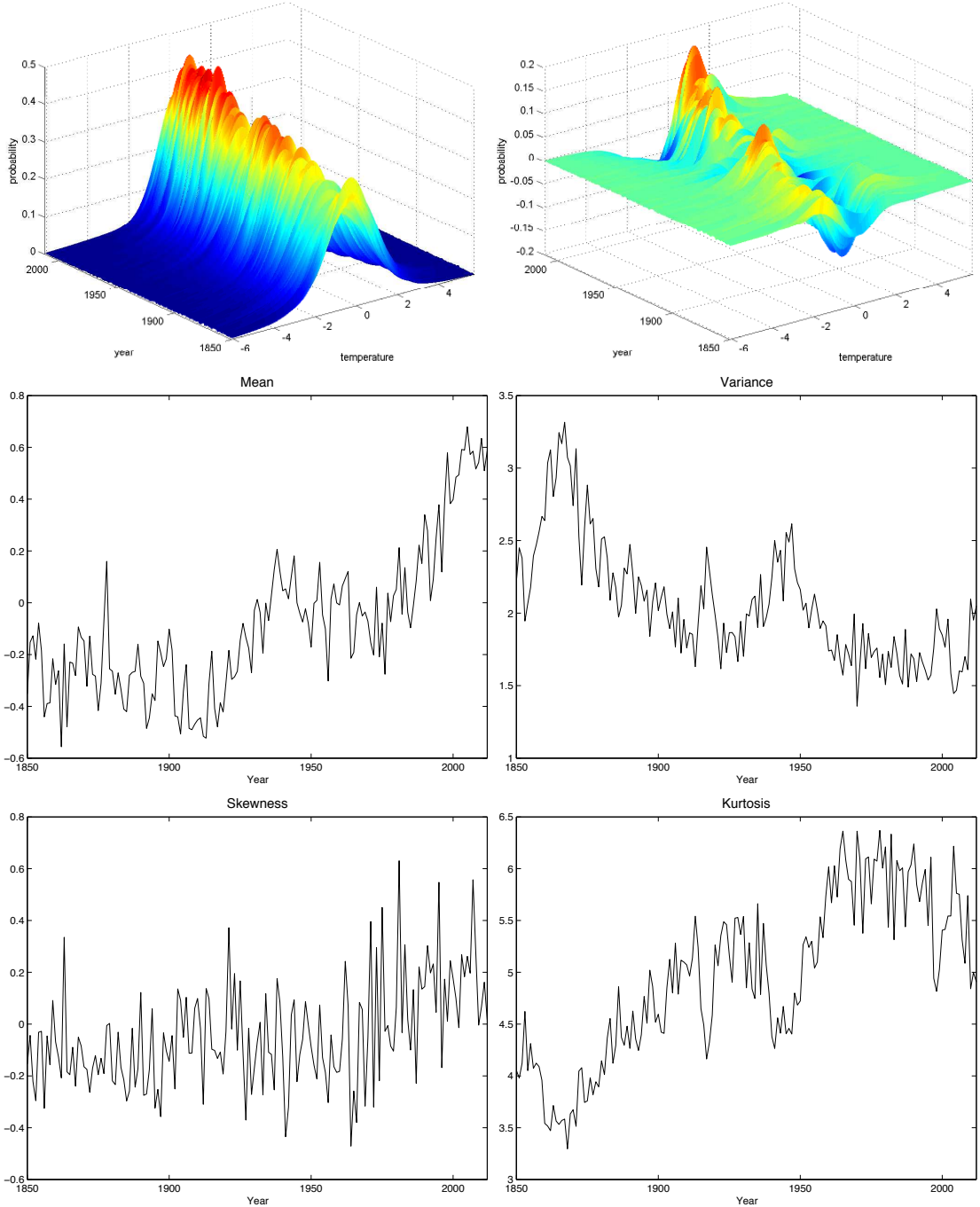


Figure 3: NH Temperature Anomaly Densities and Moments. Annual temperature anomalies measured on a 5° by 5° grid box. Undemeaned densities (top left panel) and temporally demeaned global densities (top right panel). Sample mean (middle left panel), variance (middle right panel), skewness (bottom left panel), and kurtosis (bottom right panel) of annual anomalies over time.

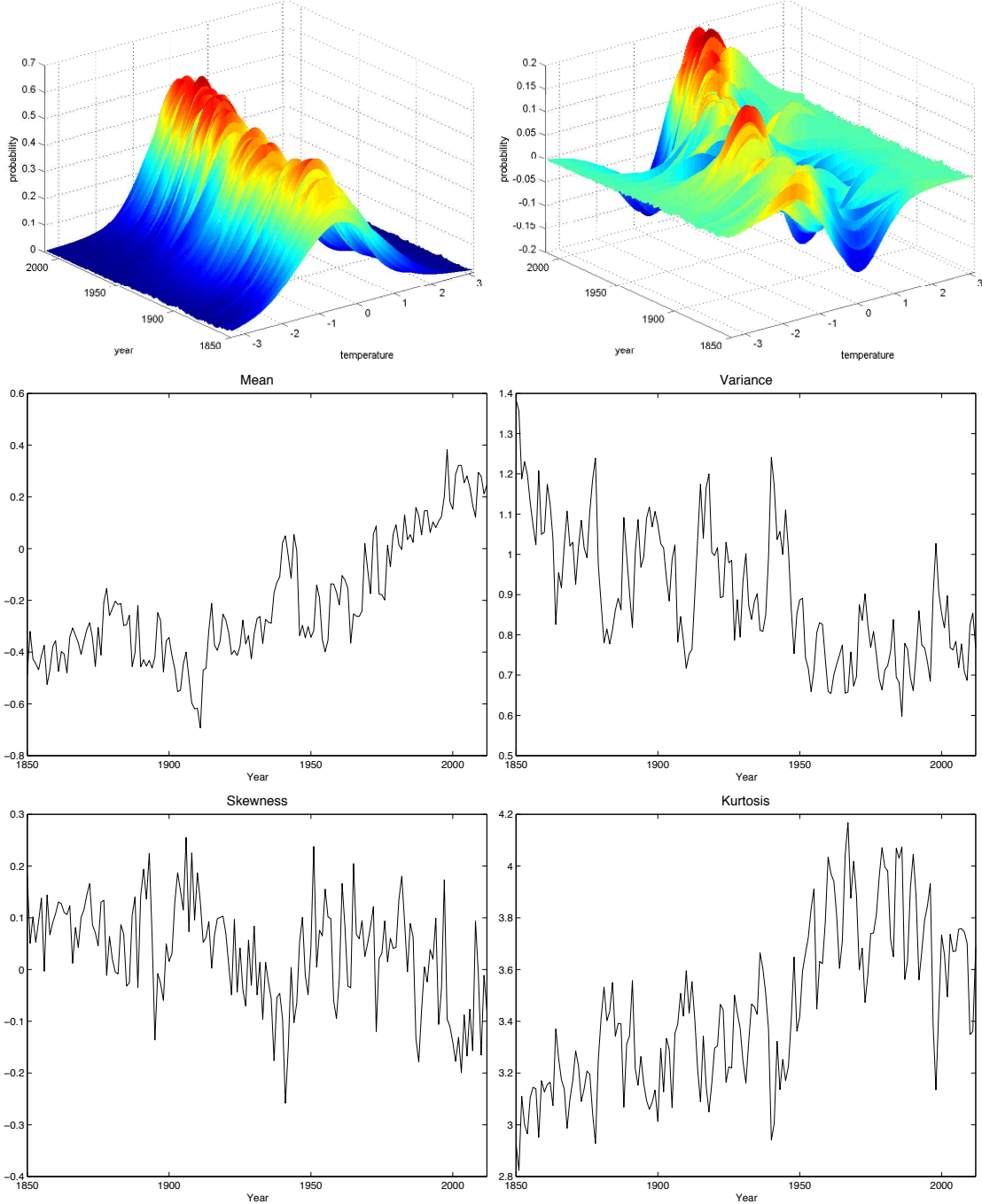


Figure 4: SH Temperature Anomaly Densities and Moments. Annual temperature anomalies measured on a 5° by 5° grid box. Undemeaned densities (top left panel) and temporally demeaned global densities (top right panel). Sample mean (middle left panel), variance (middle right panel), skewness (bottom left panel), and kurtosis (bottom right panel) of annual anomalies over time.

(middle right panels), skewnesses (bottom left panels), and kurtoses (bottom right panels) are plotted. The cross-sectional mean is defined above as $\mu_t = \int s f_t(s) ds$. Furthermore, the cross-sectional variance is given by $\sigma_t^2 = \int (s - \mu_t)^2 f_t(s) ds$, the cross-sectional skewness is given by $\tau_t^3 = \int (s - \mu_t)^3 f_t(s) ds / \sigma_t^3$ and the cross-sectional kurtosis is given by $\kappa_t^4 = \int (s - \mu_t)^4 f_t(s) ds / \sigma_t^4$ for $t = 1, \dots, T$.

Casual inspection suggests that the means have been increasing since about 1975 and perhaps since as early as 1910 in the SH, roughly consistent with the break dates identified by Gay-Garcia *et al.* (2009). While the means have increased, the skewnesses of the globe and NH are stable while that of the SH appears to have decreased from positive to negative, suggesting that although the probabilities of observing moderately positive temperature anomalies have increased, the probabilities of observing extremely positive temperature anomalies (up to the maxima of our supports) may have decreased in the SH. The variances of all the distributions appear to have decreased, suggesting a kind of global compression around the increasing mean, while the kurtoses have increased. Such movement suggests that the distributions have become more peaked around their (increasing) means, but without associated decreases in the probabilities of outliers. Instead, the probabilities of observing moderate temperature anomalies may have decreased.

In order to explore the persistence of the moments, we now turn to a more formal analysis of the stationary and nonstationary spaces of the temporally demeaned temperature anomaly densities.

2.2 Basic Framework for Time Series Analysis

We analyze the temperature densities obtained above as a time series of functional observations. As defined above, (f_t) denotes the temperature anomaly density at time t , and we define

$$w_t(s) = f_t(s) - \bar{f}_T(s) \quad (1)$$

to be the temporally demeaned temperature density for $t = 1, \dots, T$ and $s \in K$, where K is a compact subset of \mathbb{R} . Clearly, we have $\int_K f_t(s) ds = 1$ for all $t = 1, 2, \dots$, and therefore, (w_t) may be regarded as elements in the Hilbert space H given by

$$H = \left\{ w \left| \int_K w(s) ds = 0, \int_K w^2(s) ds < \infty \right. \right\}, \quad (2)$$

with inner product $\langle v, w \rangle = \int_K v(s) w(s) ds$ for $v, w \in H$.

In our analysis, we assume that the global temperature densities (f_t) are random, not deterministic, and consequently, the centered global temperatures densities (w_t) defined in

(1) become random elements taking values in the Hilbert space H , or H -valued random elements. For an introduction to random elements taking values in a Hilbert space, the reader is referred to Bosq (2000). For each $t = 1, \dots, T$, f_t is a random function and we may define its moments. In particular, we let its mean be given by the expectation $\mathbb{E}f_t$, and define its variance to be the expected tensor product $\mathbb{E}(f_t - \mathbb{E}f_t) \otimes (f_t - \mathbb{E}f_t)$ of the demeaned f_t with itself.³ The mean and variance of f_t therefore become a function and an operator respectively for $t = 1, \dots, T$. On the other hand, since each element f_t of the sequence (f_t) represents a density, we may also define its moments. We have already defined these as *cross-sectional moments* μ_t , σ_t^2 , etc., of f_t . Note that the cross-sectional moments of f_t are random variables for each $t = 1, \dots, T$.

We assume that there exists an orthonormal basis (v_i) of H such that the *i-th coordinate process* $\langle v_i, w_t \rangle$ is nonstationary, having a stochastic or deterministic trend, for each $i = 1, \dots, n$, while it is stationary for each $i \geq n + 1$.⁴ By convention, we let $n = 0$ if all of the coordinate processes are stationary. Using the symbol \bigvee to denote span, we may write $H = H_N \oplus H_S$ with

$$H_N = \bigvee_{i=1}^n v_i \quad \text{and} \quad H_S = \bigvee_{i=n+1}^{\infty} v_i,$$

which will respectively be referred to as the *nonstationary and stationary subspaces of H* . Subsequently, we define Π_N and Π_S to be the projections on H_N and H_S , and let

$$w_t^N = \Pi_N w_t \quad \text{and} \quad w_t^S = \Pi_S w_t,$$

where (w_t^N) and (w_t^S) signify respectively the nonstationary and stationary components of (w_t) . Since $\Pi_N + \Pi_S$ equals the identity operator in H , we have $w_t = w_t^N + w_t^S$.

We say that (f_t) is (weakly) stationary if it has time invariant mean and variance that are finite and well defined. In this case, we have $n = 0$, because the coordinate processes are all stationary. Under stationarity, we may expect that $\bar{f}_T(s) \approx \mathbb{E}f_t(s)$ and $w_t(s) \approx f_t(s) - \mathbb{E}f_t(s)$ for all $t = 1, \dots, T$ and $s \in K$ if T is large. Consequently, we may effectively let

$$w_t(s) = f_t(s) - \mathbb{E}f_t(s) \tag{3}$$

if T is large, in place of our definition in (1). In our subsequent analysis, we do not

³Essentially, tensor products of finite dimensional vectors yield matrices. In contrast, tensor products of functions become infinite dimensional and they are formally interpreted as operators in a Hilbert space of functions.

⁴Of course, there exists a wide variety of nonstationary processes that do not have any trends, stochastic or deterministic. In the paper, however, we only consider nonstationary processes with trends increasing either stochastically or deterministically.

distinguish between any stationary time series defined from (w_t) in (3) and (w_t) in (1).

Once we fix an arbitrary orthonormal basis (ϕ_i) of H , we may write any function w in H as a linear combination of (ϕ_i) as in $w = \sum_{i=1}^{\infty} c_i \phi_i$ with a numerical sequence (c_i) . In implementing our approach, we use an orthonormal wavelet basis (ϕ_i) to represent vectors in H as their finite linear combinations of M leading basis elements for some large M . This yields the correspondence $w \leftrightarrow (c_1, \dots, c_M)'$ between $w \in H$ and $(c_1, \dots, c_M)' \in \mathbb{R}^M$, which allows us to regard a function in H essentially as a large dimensional vector in Euclidean space. Under this convention, the inner product $\langle v, w \rangle$ becomes the usual Euclidean inner product of two vectors in \mathbb{R}^M corresponding respectively to v and w in H , and the tensor product $v \otimes w$ reduces to the conventional Euclidean outer product of two vectors in \mathbb{R}^M corresponding respectively to v and w in H .

2.3 Testing for Nonstationarity

The test for nonstationarity of the global temperature anomaly distributions we use is based on the sample operator

$$Q_T = \sum_{t=1}^T w_t \otimes w_t, \quad (4)$$

which yields the quadratic form

$$\langle v, Q_T v \rangle = \sum_{t=1}^T \langle v, w_t \rangle^2 \quad (5)$$

for any $v \in H$.

The magnitude of quadratic form (5) in $v \in H$ defined by Q_T differs primarily depending upon whether v is in H_N or in H_S . For $v \in H_S$, the coordinate process $(\langle v, w_t \rangle)$ becomes stationary and $T^{-1} \sum_{t=1}^T \langle v, w_t \rangle^2 \rightarrow_p \mathbb{E} \langle v, w_t \rangle^2$, and the quadratic form is of order T . In contrast, the magnitude of the quadratic form in $v \in H_N$ is of order bigger than T , since we assume that for all $v \in H_N$ the coordinate process $(\langle v, w_t \rangle)$ has a stochastic or deterministic trend. We may therefore extract the principle components of Q_T in (4) and use them to test for nonstationarity in the temperature anomaly distributions.

The exact magnitude of the quadratic form in $v \in H_N$ defined by Q_T further depends on the type of nonstationarity exhibited by the coordinate process $(\langle v, w_t \rangle)$. The quadratic form is of order T^2 if the coordinate process has unit root nonstationarity (a stochastic trend). On the other hand, it is of order T^3 if the coordinate process has a linear deterministic trend, and it diverges at an exponential rate if the coordinate process has an explosive root.

To identify these different types of nonstationarity in the global temperature distributions, we define the unit root subspace H_U of H to be the m -dimensional sub-subspace of

the n -dimensional subspace H_N such that $(\langle v, w_t \rangle)$ is a unit root process for all $v \in H_U$. For completeness, we also define the deterministic and explosive subspace H_X of H such that $H_N = H_U \oplus H_X$ and $H = H_S \oplus H_U \oplus H_X$. There is no unit root nonstationarity if $m = 0$, whereas the entire nonstationarity is unit root nonstationarity if $m = n$. In fact, we find that $m = n$ in our empirical results on temperature anomalies below. However, we also consider the case of $m < n$ here to introduce our test to distinguish between these cases.

Denote by $v_1(Q_T), v_2(Q_T), \dots$ the orthonormal eigenvectors of operator Q_T in (4) with associated eigenvalues $\lambda_1(Q_T) \geq \lambda_2(Q_T) \geq \dots$. It follows that

$$\lambda_i(Q_T) = \langle v_i(Q_T), Q_T v_i(Q_T) \rangle = \sum_{t=1}^T \langle v_i(Q_T), w_t \rangle^2.$$

Therefore, it is natural to estimate H_N by the span of $v_1(Q_T), \dots, v_n(Q_T)$ – i.e., n orthonormal eigenvectors of Q_T associated with the n largest eigenvalues of Q_T . Chang *et al.* (2016) establish the consistency of the estimator for the case in which we only have unit root nonstationarity. Extending their proof to allow for more general types of nonstationarity is straightforward. In our setup, if normalized by T^2 , $\lambda_{n-m+1}(Q_T), \dots, \lambda_n(Q_T)$ have well defined limit distributions as $T \rightarrow \infty$, while $\lambda_1(Q_T), \dots, \lambda_{n-m}(Q_T)$ diverge faster than the rate T^2 . In particular, the unit root subspace H_U can be estimated consistently by the span of m -orthonormal eigenvectors $v_{n-m+1}(Q_T), \dots, v_n(Q_T)$ of Q_T .

We find the values of n and m by successive testing procedures for the null hypothesis of unit root nonstationarity against the alternative hypothesis of stationarity, and then against the alternative hypothesis of deterministic/explosive nonstationarity. We expect the eigenvalues $(\lambda_i(Q_T))$ to have discriminatory powers for such tests. However, they cannot be used directly, because their limit distributions are dependent upon nuisance parameters. Therefore, we construct tests based on eigenvalues with limit distributions free of nuisance parameters.

To this end, we define (z_t) by either

$$z_t = (\langle v_1(Q_T), w_t \rangle, \dots, \langle v_p(Q_T), w_t \rangle)' \quad (6)$$

(v_p is the eigenvector associated with the p -th largest eigenvalue) or

$$z_t = (\langle v_{n-q+1}(Q_T), w_t \rangle, \dots, \langle v_n(Q_T), w_t \rangle)' \quad (7)$$

(v_n is the eigenvector in H_N associated with the smallest eigenvalue) for $t = 1, \dots, T$, and we use the index r to denote p or q depending upon whether (z_t) is given by (6) or (7). Moreover, we define the product sample moment $Q_r^T = \sum_{t=1}^T z_t z_t'$, and the long-run variance estimator

τ_p^T	$p = 1$	2	3	4	5
1%	0.0274	0.0175	0.0118	0.0103	0.0085
5%	0.0385	0.0223	0.0154	0.0127	0.0101
10%	0.0478	0.0267	0.0175	0.0139	0.0111
σ_q^T	$q = 1$	2	3	4	5
99%	0.7487	1.0073	1.2295	1.4078	1.5952
95%	0.4660	0.6787	0.8645	1.0336	1.1892
90%	0.3494	0.5399	0.7066	0.8574	1.0092

Table 1: One-sided Critical Values for the Test Statistics τ_p^T and σ_q^T .

$\Omega_r^T = \sum_{|k| \leq \ell} \varpi_\ell(k) \Gamma_T(k)$ of (z_t) , where ϖ_ℓ is the weight function with bandwidth parameter ℓ and Γ_T is the sample autocovariance function defined as $\Gamma_T(k) = T^{-1} \sum_t \Delta z_t \Delta z'_{t-k}$.

Our test statistics are given by

$$\tau_p^T = T^{-2} \lambda_{\min}(Q_p^T, \Omega_p^T) \quad (8)$$

and

$$\sigma_q^T = T^{-2} \lambda_{\max}(Q_q^T, \Omega_q^T), \quad (9)$$

where $\lambda_{\min}(Q_p^T, \Omega_p^T)$ and $\lambda_{\max}(Q_q^T, \Omega_q^T)$ are respectively the smallest and the largest generalized eigenvalues of Q_r^T with respect to Ω_r^T for $r = p$ or q .

The test statistics τ_p^T and σ_q^T introduced in (8) and (9) are used with the critical values obtained under the null hypothesis that (z_t) defined in (6) or (7) is a unit root process in order to determine n and m . Under very general conditions, Chang *et al.* (2016) show that the statistic τ_p^T has a well-defined nondegenerate limit distribution that is free of nuisance parameters and depends only on p , as long as $n - m + 1 \leq p \leq n$ (for $m, n \geq 1$). We may extend their result and establish that it is also true for the statistic σ_q^T under the same conditions if $1 \leq q \leq m$ (for $m, n \geq 1$). We compute the critical values of the new statistic σ_q^T up to $q = 5$ (Table 1) together with the critical values of the statistic τ_p^T for easy reference.

Note that the statistic τ_p^T converges to 0 for all $p > n$. Therefore, we may use τ_p^T to determine n as follows.⁵ We start from a value of p large enough to be bigger than n and test the null hypothesis $H_0 : \dim(H_N) = p$ against the alternative hypothesis $H_1 : \dim(H_N) \leq p - 1$ successively downward, until we reach $p = 1$. For each test, we reject the null hypothesis if the value of τ_p^T is *smaller* than the respective critical values provided

⁵Our testing procedure here is entirely analogous to the sequential procedure in Johansen (1995), which is commonly used to determine the cointegration ranks in error correction models.

in Table 1. We proceed as long as we reject the null hypothesis in favor of the alternative hypothesis, and set our estimate for n to be the largest value p_{\max} , for which we fail to reject the null hypothesis. Because this successive testing procedure employs a consistent test, it allows us to find the true value of n with asymptotic probability of virtually one by making the size of the test small enough.

Once n is found, we may use the statistic σ_q^T to determine m . Note that the statistic σ_q^T diverges to infinity for all $m < q \leq n$. We start from $q = n$ and test the null hypothesis $H_0 : \dim(H_U) = q$ against the alternative hypothesis $H_1 : \dim(H_U) \leq q - 1$ successively downward, until we reach $q = 1$. For the test, we reject the null hypothesis if σ_q^T takes a value *larger* than the respective critical value reported in Table 1, in contrast to the test based on τ_p^T . As above, we proceed as long as the null hypothesis is rejected in favor of the alternative hypothesis and set our estimate for m to be the largest value q_{\max} of q , for which we fail to reject the null hypothesis. Again, this procedure allows us to find the true value of m with asymptotic probability arbitrarily close to one.

2.4 Nonstationarity in Cross-Sectional Moments

Once we determine n and estimate the nonstationary subspace H_N , we may determine the nonstationary proportion of each cross-sectional moment. Similarly to Chang *et al.* (2016), we define a function

$$\mu_i(s) = s^i - \frac{1}{|K|} \int_K s^i ds$$

for $i = 1, 2, \dots$ and Lebesgue measure $|K|$ of K , and note that

$$\langle \mu_i, w_t \rangle = \langle \mu_i, f_t \rangle - \mathbb{E}\langle \mu_i, f_t \rangle$$

represents the fluctuations over time of the i -th moments of the distributions with densities (f_t) around their expected values.

The function μ_i may be decomposed as $\mu_i = \Pi_N \mu_i + \Pi_S \mu_i$ with Π_N and Π_S defined as projections respectively on the nonstationary and stationary subspaces H_N and H_S , so that

$$\|\mu_i\|^2 = \|\Pi_N \mu_i\|^2 + \|\Pi_S \mu_i\|^2 = \sum_{j=1}^n \langle \mu_i, v_j \rangle^2 + \sum_{j=n+1}^{\infty} \langle \mu_i, v_j \rangle^2, \quad (10)$$

where (v_j) for $j = 1, 2, \dots$ is an orthonormal basis of H such that $(v_j)_{1 \leq j \leq n}$ spans H_N and $(v_j)_{j \geq n+1}$ spans H_S .

The proportion of the component of μ_i lying in H_N is given by

$$\pi_i^N = \frac{\|\Pi_N \mu_i\|}{\|\mu_i\|} = \sqrt{\frac{\sum_{j=1}^n \langle \mu_i, v_j \rangle^2}{\sum_{j=1}^\infty \langle \mu_i, v_j \rangle^2}} \quad (11)$$

with the convention that $\pi_i^N = 0$ when $n = 0$ (μ_i is entirely in H_S). On the other hand, μ_i is entirely in H_N if $\pi_i^N = 1$. π_i^N represents the proportion of the nonstationary component in the i -th moment, which we call the *nonstationary proportion* of the i -th moment. As π_i approaches zero, the i -th moment is predominantly stationary, but it is predominantly nonstationary as π_i tends to unity.

To supplement π_i^N , we propose a new ratio given by

$$\pi_i^U = \frac{\|\Pi_U \mu_i\|}{\|\mu_i\|} = \sqrt{\frac{\sum_{j=n-m+1}^n \langle \mu_i, v_j \rangle^2}{\sum_{j=1}^\infty \langle \mu_i, v_j \rangle^2}}, \quad (12)$$

where Π_U is the projection on the unit root subspace H_U , with the convention that $\pi_i^U = 0$ when $m = 0$. When $m = n$, $\pi_i^U = \pi_i^N$ so that the component of μ_i in H_N is entirely in H_U . Alternatively, when $m = 0$ and $\pi_i^U = 0$, all of the proportion in H_N is in the deterministic and explosive subspace H_X . We call π_i^U the *unit root proportion* of the i -th moment. Generally, it is more difficult to predict the i -th moment if π_i^U is closer to unity. In contrast, the i -th moment is easier to predict if π_i^U is small – either because $\|\Pi_S \mu_i\|$ is relatively large due to stationarity or because $\|(\Pi_N - \Pi_U) \mu_i\|$ is relatively large due to a deterministic trend.

3 Persistent Features in Temperature Anomalies

We now discuss how to implement the tests and create the proportions discussed above using actual data, and we present the results for the temperature anomaly distributions. We then show unit root proportions and graphical representations of the stationary and nonstationary components.

3.1 Empirical Implementation of the Tests and Proportions

To implement our methodology, use the cross-sectional densities that we regard as functional observations on the Hilbert space H introduced in (2). In our analysis, H is assumed to have a countable basis. This implies that any $w \in H$ can be represented as an infinite linear combination of the basis elements, and that the representation is unique. Therefore, there is a one-to-one correspondence between H and \mathbb{R}^∞ and the correspondence is uniquely

defined, once the basis elements are fixed.

For instance, once a basis (ϕ_1, ϕ_2, \dots) is given, we may write any $w \in H$ as $w = c_1\phi_1 + c_2\phi_2 + \dots$ and the correspondence becomes $w \leftrightarrow (c_1, c_2, \dots)$. We use this correspondence in our analysis of functional observations. Of course, the correspondence becomes operational only if we replace \mathbb{R}^∞ by \mathbb{R}^M for some large M . Subsequently, we let $[w] = (c_1, \dots, c_M)'$ and define a correspondence

$$w \leftrightarrow [w] \quad (13)$$

between H and \mathbb{R}^M in place of \mathbb{R}^∞ . In our analysis, we use a Daubechies wavelet basis and set $M = 1,037$, which we believe to be sufficiently large.

Under the correspondence between H and \mathbb{R}^M defined in (13), we have the correspondences

$$\langle v, w \rangle \leftrightarrow [v]'[w] \quad \text{and} \quad v \otimes w \leftrightarrow [v][w]'$$

for any $v, w \in H$. In fact, under the correspondence in (13), the linear operator Q on H defined in (4) generally corresponds to a square matrix of dimension M denoted by $[Q]$, and we have in particular

$$\langle v, Qw \rangle \leftrightarrow [v]'[Q][w]$$

for any $v, w \in H$. We use these correspondences throughout our analysis.

For ease of reference and clarity of exposition, and because our procedure is new, we briefly outline seven steps utilized to create the test statistics τ_p^T and σ_q^T using actual data from a finite sample.

1. **Obtain w_t .** We regard w_t as an M -dimensional vector $[w_t]$ for each t .
2. **Create Q_T .** Implement $Q_T = \sum_{t=1}^T w_t \otimes w_t$ as $[Q_T] = \sum_{t=1}^T [w_t][w_t]'$ for each t .
3. **Calculate $v_i(Q_T)$.** We identify these as $[v_i(Q_T)]$, which are M orthonormal eigenvectors of the M -dimensional square matrix $[Q_T]$.
4. **Create z_t from (6) or (7).** Inner products $\langle v_i(Q_T), w_t \rangle$ are computed as $[v_i(Q_T)]'[w_t]$ for each i and t .
5. **Create Q_r^T and Ω_r^T .** Implement $Q_r^T = \sum_{t=1}^T z_t z_t'$ and $\Omega_r^T = \sum_{|k| \leq \ell} \varpi_\ell(k) \Gamma_T(k)$ using the Parzen window with Andrews plug-in bandwidth.
6. **Calculate $\lambda(Q_r^T, \Omega_r^T)$.** These are generalized eigenvalues of Q_r^T with respect to Ω_r^T for $r = p$ or q .
7. **Calculate Test Statistics τ_p^T from (8) and σ_q^T from (9).**

$p, q =$		1	2	3	4
Global	τ_p^T	0.0637	0.0297	0.0116	0.0116
	σ_q^T	0.0637	0.0727		
NH	τ_p^T	0.0497	0.0425	0.0125	0.0120
	σ_q^T	0.0497	0.0680		
SH	τ_p^T	0.0654	0.0203	0.0096	0.0085
	σ_q^T	0.0654			

Table 2: **Test Statistics** τ_p^T and σ_q^T . Global, NH, and SH temperature anomaly distributions.

Once these test statistics have been calculated, the ranks of the respective spaces are chosen using the sequential procedure described above.

The nonstationary and unit root proportions of the i -th moment defined in (11) and (12) cannot be calculated directly, since H_N and H_U are unknown. Instead, we may use the *sample* nonstationary and unit root proportions of the i -th cross-sectional moment

$$\hat{\pi}_{iT}^N = \sqrt{\frac{\sum_{j=1}^n \langle \mu_i, v_j(Q_T) \rangle^2}{\sum_{j=1}^M \langle \mu_i, v_j(Q_T) \rangle^2}} \quad \text{and} \quad \hat{\pi}_{iT}^U = \sqrt{\frac{\sum_{j=n-m+1}^n \langle \mu_i, v_j(Q_T) \rangle^2}{\sum_{j=1}^M \langle \mu_i, v_j(Q_T) \rangle^2}} \quad (14)$$

to estimate π_i^N and π_i^U . Chang *et al.* (2016) show that the sample nonstationary proportion $\hat{\pi}_{iT}^N$ is a consistent estimator of the original nonstationary proportion π_i^N , and by extension $\hat{\pi}_{iT}^U$ is a consistent estimator of π_i^U .

3.2 Tests Statistics

Table 2 shows the τ_p^T and σ_q^T test statistics for the global, NH, and SH temperature anomalies up to $p = 4$. Starting with τ_p^T for the global distribution and comparing the statistic with the critical values in Table 1 we reject $p = 4$ against the alternative $p \leq 3$, and then we reject $p = 3$ against the alternative $p \leq 2$, both with a size of 5% or less. We cannot reject $p = 2$ against $p \leq 1$ even with 10%. We obtain the same results for the NH distribution. For the SH, $p = 4$ and $p = 3$ are strongly rejected at 1% size, $p = 2$ is rejected at 5% size, but $p = 1$ is not rejected against $p = 0$.

We therefore choose the dimension of the nonstationary subspace $\dim(H_N)$ to be $n = 2$ for the NH and the globe, but $n = 1$ for the SH. We may interpret the nondegenerate dimension of the nonstationary subspace to mean that all three series of distributions have some persistence that is strong enough to be *permanent* in the sense that shocks to the temperature anomaly distributions accumulate over time. Changes in the temperature anomaly distributions are not entirely *transitory*.

	$\hat{\pi}_{1T}^N$	$\hat{\pi}_{2T}^N$	$\hat{\pi}_{3T}^N$	$\hat{\pi}_{4T}^N$	$\hat{\pi}_{5T}^N$	$\hat{\pi}_{6T}^N$	$\hat{\pi}_{7T}^N$
Global	0.303	0.214	0.085	0.083	0.044	0.046	0.030
NH	0.293	0.199	0.088	0.077	0.051	0.045	0.038
SH	0.448	0.154	0.173	0.078	0.094	0.050	0.064

Table 3: **Sample Nonstationary Proportions in the First Seven Moments.** Global, NH, and SH temperature anomaly distributions.

Is the persistence of the unit root type, or is the persistence explosive or deterministic? To answer this question, we now examine σ_q^T . Looking first at the global distribution, $q = n = 2$ is not rejected at any reasonable significance level against $q \leq 1$, and neither is $q = 1$ against $q = 0$. We thus choose $\dim(H_U)$ to be $m = n = 2$ for the global distribution. The same outcome $m = n = 2$ is obtained for the NH, while that for the SH is similarly $m = n = 1$. The fact that $m = n$ is chosen in every case suggests that all of the nonstationarity is better characterized by unit-root-type persistence, which suggests stochastic trends are present in the moments of the distributions, than by higher-order persistence, which would suggest explosive roots or linear deterministic trends.

3.3 Estimated Proportions

We now turn to the proportions of the subspaces defined above in each cross-sectional moment of temperature anomalies. Note that we set $\pi_i^U = \pi_i^N$ – i.e., the unit root space spans the entire nonstationary space – because we do not find evidence of any higher-order persistence. Table 3 shows consistent estimates $\hat{\pi}_{iT}^N$ for $i = 1, \dots, 7$ of the proportion of the nonstationary subspace π_i^N in each of the first seven cross-sectional moments of temperature anomalies. The remaining proportions are in the stationary subspace π_i^S .

Roughly a third (30.3%) of the persistence in the mean global mean is strong enough to be unit-root-type persistence. The persistence in the mean appears to be stronger in the SH than the NH, in the sense that 44.8% of the persistence in the Southern mean is of the unit root type, while only 29.3% of that north of the Equator. The global, NH, and SH variances are 21.4%, 19.9%, and 15.4% respectively, which suggests that nonstationary proportions in the variance are lower than those in the mean and roughly similar in both hemispheres.

The proportion of unit root persistence in the skewness for the globe is 8.5%. Like the mean, the skewness appears to be less persistent in the NH (8.8%) than in the SH (17.3%). Persistence appears to decline in the remaining four moments for the globe and NH, while it remains roughly 5-9% in the SH.

3.4 Estimated Components

Because the concepts of stationarity and nonstationarity of densities are quite new, we present some further illustrations of these components. The left panels of Figure 5 show the time series of demeaned densities (w_t) (same as the top right panels of Figures 2-4) for the globe, NH, and SH. The right panels show the time series of stationary components of the respective densities (w_t^S). These are calculated by subtracting the estimated nonstationary (unit root) components (w_t^N), calculated as $w_t^N = \Pi_N w_t$, from the densities (w_t). Recall that the dimension of n ($= m$) is estimated to be two for the globe and NH and one for the SH. In all three cases – but especially in the first two – the stationary components of the densities appear to be more like random noise, showing very little evidence of persistence in any of the moments. Evidently, the temporal patterns in the densities are driven by their nonstationary components rather than by their stationary components.

The concept of nonstationarity will be more familiar to readers in a simple time series context. To this end, Figure 6 shows the nonstationary components more clearly. First, we plot the normalized mean process. The mean process is given by μ_t above (middle left panels of Figures 2-4), but we normalize the series to unit length with a Euclidean norm since the eigenvectors used to compute the nonstationary coordinate processes have unit length. We then plot the two estimated nonstationary coordinate processes $\langle v_1, w_t \rangle$ and $\langle v_2, w_t \rangle$ – which could be written as (c_{1t}) and (c_{2t}) using the correspondence in (13) – for the globe and NH and the one $\langle v_1, w_t \rangle$ for the SH.

Clearly, the estimated nonstationary coordinate processes exhibit more persistence compared to the time series of cross-sectional means that include both stationary and nonstationary components. In other words, the time series plots of the nonstationary coordinate processes better resemble sample paths of unit root processes than those of stationary processes – or those of trend stationary processes, for that matter. We see stronger evidence for the globe and NH, but less so for the SH, which is not surprising given that we have only a one-dimensional unit root space for the SH and the unit root proportion of the mean process is nearly 45%, which captures a substantial portion of nonstationarity in the time series of SH temperature distributions.

4 Discussion of the Empirical Findings

A more in-depth discussion of our empirical results follows. Specifically, we link the detected persistence in the moments of the global and hemispheric distributions to findings in the extant literature on anthropogenic hemispheric differences, changes in record temperatures, and the observed slowdown in global warming since the late 1990's.

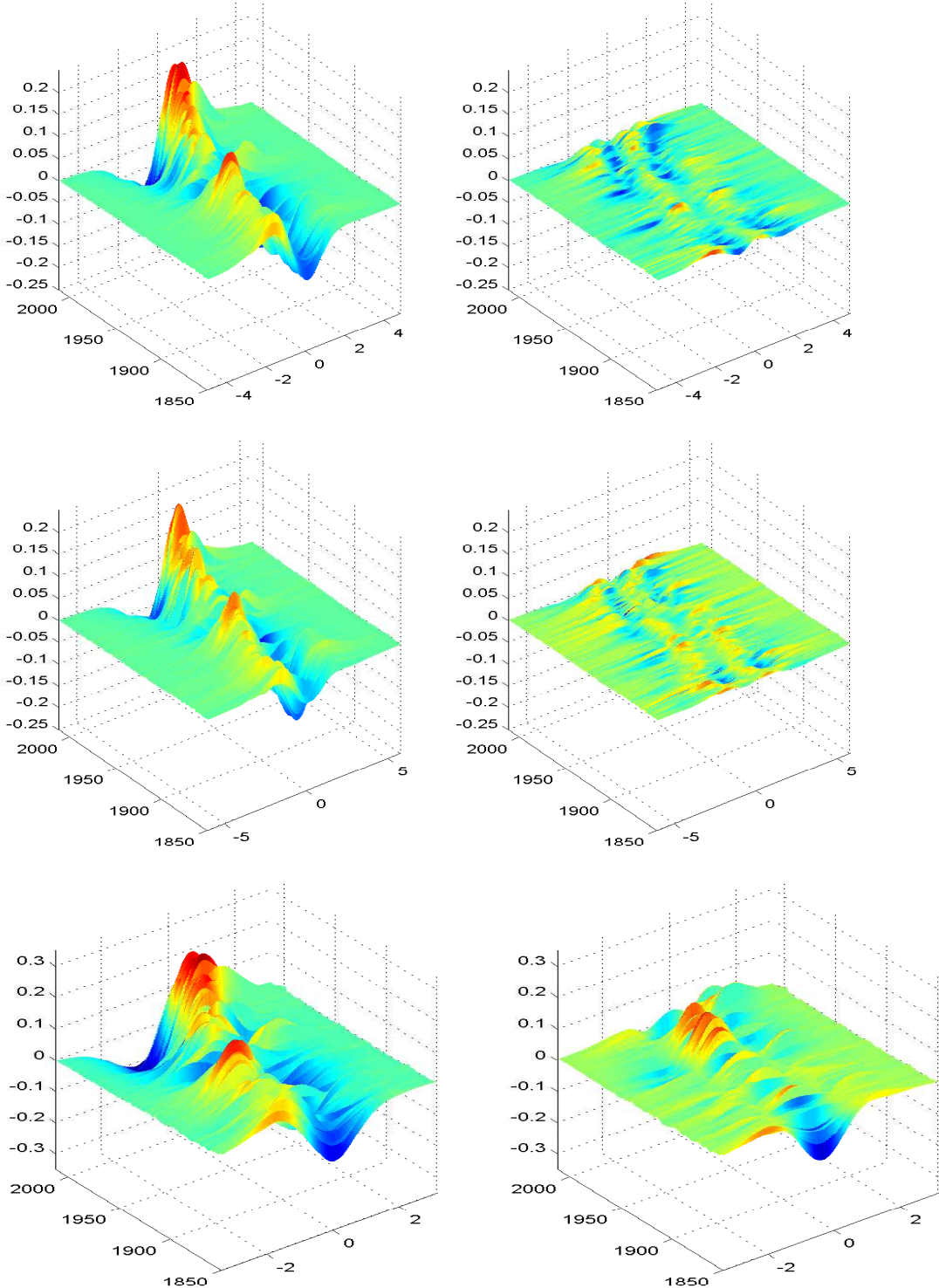


Figure 5: Densities and Stationary Components. Temporally demeaned densities (w_t) (left) and stationary components (w_t^S) (right) for the globe (top), NH (middle), and SH (bottom).

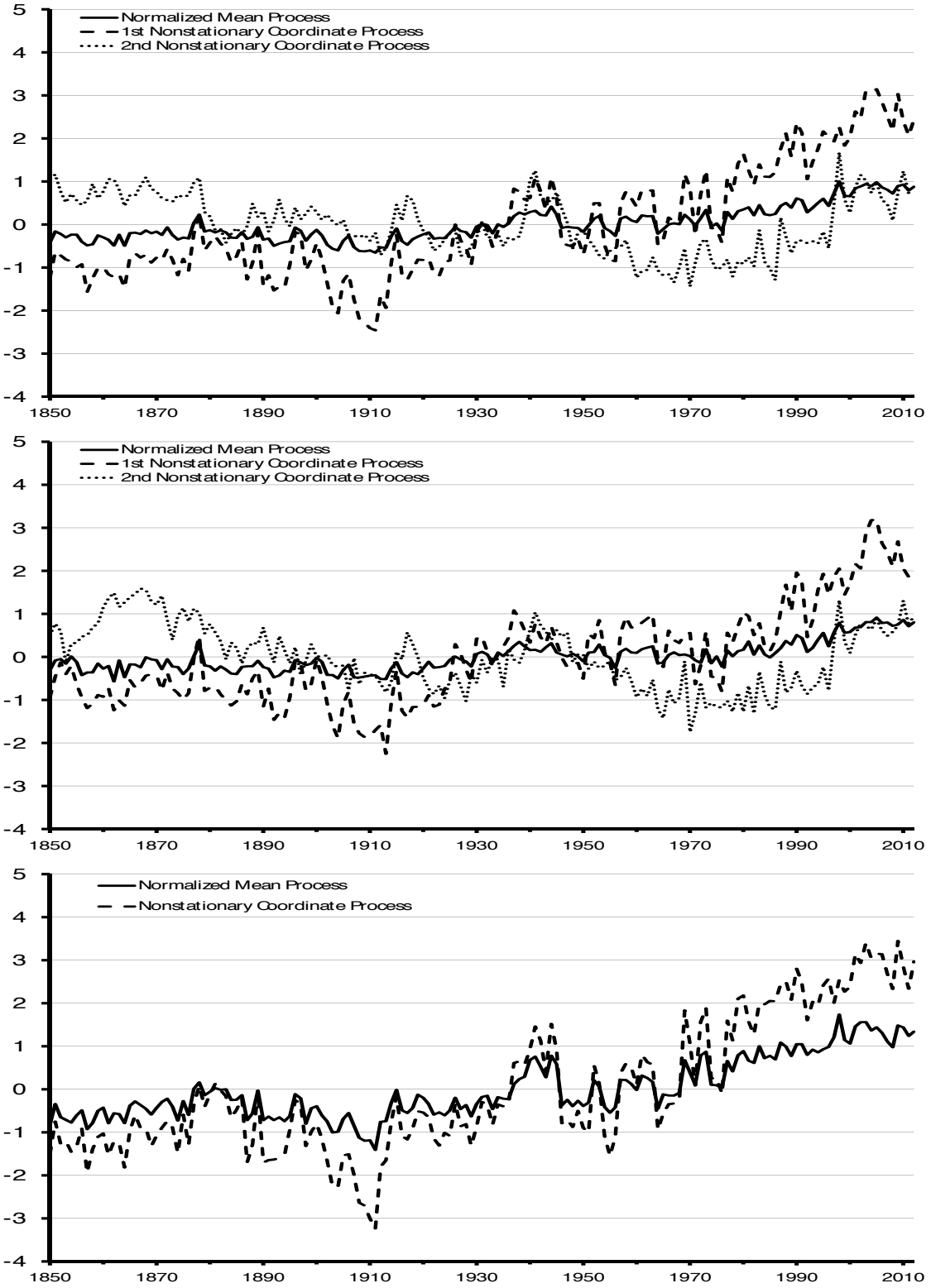


Figure 6: Mean and Nonstationary Components. Normalized mean processes and estimated nonstationary coordinate processes for the globe (top), NH (middle), and SH (bottom). The coordinate processes are identified up to sign. We set their signs so that the processes move in the same direction as the mean processes.

4.1 Attribution to Hemispheric Differences in Human Activity

The estimated nonstationary coordinate processes clearly illustrate strong persistence in the distributions. However, our results generally are inconsistent with the hypothesis that temperature contains a deterministic trend, with or without a break. In other words, the time series plots of the nonstationary coordinate processes better resemble sample paths of unit root processes than those of stationary process or those of trend stationary processes.

Instead, the persistence of mean temperature is consistent with the hypothesis that changes in temperature are generated by a stochastic trend. The presence of a stochastic trend does not mean that temperature follows a random walk, as Gordon (1991) argues. A random walk is a very special case of a unit root process that has completely unpredictable increments. Instead, a unit root process may have increments with strong but stationary persistence, which indicates that changes in the global mean temperature may have long-lasting effects. Such persistent changes yield a stochastic trend that may indeed increase over long periods, which gives the appearance of a linear or broken trend.

The presence of a stochastic trend is consistent with the anthropogenic theory of climate change. According to this hypothesis, the stochastic trends in mean temperatures originate from stochastic trends in radiative forcing. These stochastic trends in forcing come from stochastic trends in the capital stock, which emits greenhouse gases and sulfur, and from their long residence times, which means that the atmosphere integrates emissions into radiative forcing.

The effect of stochastic trends in radiative forcings on surface temperature is consistent with hemispheric differences in the persistence of temperature anomalies and the number of nonstationary coordinate processes. As indicated in Table 3, the persistence of the mean temperature for the Southern Hemisphere appears stronger than persistence in the mean temperature for the Northern Hemisphere. Nearly 45% of the persistence in the Southern mean is of the unit root type, while only 29.3% is of the unit root type north of the Equator. With regard to nonstationary coordinate processes, there are two in the NH; the SH contains only one (Figure 6).

We postulate that these hemispheric differences are generated by a natural experiment in which most of the human population and its economic activity is located in the NH. Under these conditions, the NH is the locus for the greatest emissions of greenhouse gases, such as carbon dioxide, methane, nitrous oxide, and CFC's. These gases have a relatively long residence time: decades to centuries (Ramaswamy *et al.*, 2001). Their long residence time means that the atmosphere integrates the stochastic trend in greenhouse gas emissions (due to the stochastic trend in capital stock) such that the radiative forcing of greenhouse gases appears is highly persistent (Stern and Kaufmann, 2000; Kaufmann *et al.*, 2006).

Furthermore, these long residence times imply that the concentrations of greenhouse gas (and their forcings) are relatively well mixed across the hemispheres. For example, the average concentration of CO₂ at Barrow, Alaska (71.3230° North, 156.6114° West) in 2014 was 400 ppm; it was 395 ppm at Cape Point, South Africa (34.3523° South, 18.4891° East) (<http://www.esrl.noaa.gov/gmd/>).

Similarly, the NH is the locus for the highest rate of anthropogenic sulfur emissions. But these emissions have a relatively short lifetime in the atmosphere, about a week to ten days (Shine *et al.*, 1991). This short residence time implies that the atmosphere does not integrate the stochastic trend in anthropogenic sulfur emissions that is imparted by long-lived capital stock. As a result, univariate tests indicate that the radiative forcing due to anthropogenic sulfur emissions is less persistent than the radiative forcing of greenhouse gases (Stern and Kaufmann, 2000; Kaufmann *et al.*, 2006). The short residence times also means that anthropogenic sulfur emissions are not mixed thoroughly across the hemispheres; the annual mean for the direct radiative forcing of anthropogenic sulphates in the NH is 2-7 times greater than in the SH (Ramaswamy *et al.*, 2001). As a result, the cooling effects of anthropogenic sulfur emissions are strongest in the NH, with relatively little effect in the SH.

These hemispheric differences in radiative forcing are consistent with results that identify one nonstationary coordinate process in the SH and two nonstationary coordinate processes in the NH. The first nonstationary coordinate component is similar in both hemispheres. We interpret these processes to be the persistent movements that are caused by the radiative forcing of greenhouse gases. Beyond the similarity of forcings across hemispheres, this interpretation is supported by movements over time. In general, the radiative forcing of greenhouse gases starts its rapid increase in the 1970's (Kaufmann *et al.*, 2011), which is consistent with the increases in the first global nonstationary coordinate process in Figures 6.

We interpret the second nonstationary component in the NH as driven by the radiative forcing of anthropogenic sulfur emissions. These emissions have a cooling effect, which is consistent with the general decline shown in Figure 6. Consistent with this interpretation, the second nonstationary coordinate process in Figure 6 reaches a trough in the mid 1970's. After this point, legislation aimed at reducing acid deposition in North America, Europe, and Japan reduces sulfur emissions, which reduces their cooling effect. Lower rates of cooling are consistent with a rise in the second nonstationary coordinate process that starts in the 1980's. The direction of these movements and their interpretation are similar to a structural time series analysis of hemispheric temperatures (Stern and Kaufmann, 2000).

Because of the differences in radiative forcing across the Equator, the warming effect of

enhanced forcing due to greenhouse gases is strongest in the SH; in the NH, the warming is offset by the cooling effect of anthropogenic sulfur emissions. In some areas of the NH, such as Southeast Asia and parts of Europe, anthropogenic sulfur emissions reduce total forcing relative to pre-industrial levels (Myhre *et al.*, 2013). These spatial variations in forcing are important because they affect local rates of temperature change (Magnus *et al.*, 2011).

Under these conditions, persistence is greatest in the SH because temperatures embody the highly persistent warming effects of greenhouse gas forcing alone. Temperature changes in the NH are less persistent because the highly persistent warming is offset by the cooling that is caused by anthropogenic sulfur emissions.

This mechanism also can account for hemispheric differences in the change in the skewness of temperature. The larger forcing over the SH increases the likelihood of observing new records for high temperature, which is reflected by the change from a positive to negative skewness. Conversely, the smaller increases in forcing and the net reduction in some areas means that new records for high temperature are less likely. Consistent with this reduced probability, skewness changes little for NH temperatures.

4.2 Temperature Changes and Temperature Extremes

In a stationary climate, the number of new record high temperatures should be about equal to the number of new record low temperatures when averaged over several years (Lewis and King, 2015). But if average surface temperature is rising, as described by a stochastic trend (as indicated here) or a deterministic trend, the number of new record high temperatures is expected to be greater than the number of record low temperatures. As such, changes in temperature extremes are an important means of detecting climate change and evaluating the effect of climate change on human well-being.

Changes in the number of record temperatures, the size of extreme events, and the balance between the number of record high and record low temperatures are determined by (a) changes in mean temperature, (b) its effect on the probability of extreme events, and (c) the degree to which these events are skewed. We measure persistence in these three changes. The means and kurtoses of global and hemispheric temperature anomalies appear to be increasing. By itself, increases in mean temperature increase the number of new record high temperatures relative to the number of record low temperatures (Wergen and Krug, 2010).

Conversely, the increased sharpness of the peak in the frequency-distribution curve for temperature anomalies (i.e. increased kurtosis) suggests that the probabilities of observing moderately positive temperature anomalies have increased, but the probabilities of observing extremely positive temperature anomalies has decreased. If correct, this would allay

some concern about the effect of large temperature extremes on ecological or economic systems.

Finally, the skewness of the temperature anomalies declines strongly in the SH, but it is more stable in the NH. This change implies that the likelihood of new record high temperatures increases relative to the likelihood of new record low temperatures (beyond the effect of an increase in mean temperature). This result is consistent with a findings that the ratio of new record high temperatures to new record low temperatures increases faster than the increase in mean temperature (Beniston, 2015) and that record highs have dramatically outnumbered record lows in Australia since 2000 (Lewis and King, 2015).

4.3 Potential Changes in Warming and the Hiatus

Some analysts argue that the observational record temperature can be modeled using a deterministic trend, with or without a break. A break represents a period when the rate of temperature change increases (or decreases) relative to the previous period. If present, the most notable of these changes would be the so-called hiatus, which is a period during which the observed increase in temperature slows. This period is supposed to have started in the late 1990's and continues through the present (Easterling and Wehner, 2009).

To establish whether the hiatus is a statistically meaningful slow-down in warming, as opposed to a spurious outcome that is generated by an iterative search, temperature data must be analyzed using change-point techniques. These methods are designed to avoid the tendency to find a change during an iterative search that is undertaken when the presence/timing of a change is not known *a priori* (Christiano, 1992). To date, these methods are not able to identify changes that coincide with the hiatus (Cahill *et al.*, 2015; Rajaratnam *et al.*, 2015). Similarly, simulations that suggest the hiatus is caused by a sudden change in heat uptake in the southern Pacific Ocean (Kosaka and Xie, 2013) are undermined by a change-point analysis (Pretis *et al.*, 2015).

Our results, too, are inconsistent with the hypothesis of a hiatus in warming and the explanation that a sudden change in ocean uptake of heat is responsible. First our results do not support the notion that temperature changes can be described by a deterministic trend. Looking first at the global distribution, $q = n = 2$ is not rejected at any reasonable significance level against $q = 1$, and neither is $q = 1$ against $q = 0$. We thus choose $\dim(H_U)$ to be $m = n = 2$ for the global distribution. The same outcome $m = n = 2$ is obtained for the NH, while that for the SH is similarly $m = n = 1$. The fact that $m = n$ is chosen in every case suggests that all of the nonstationarity is better characterized by unit-root-type persistence, which suggests stochastic trends in the moments of the distributions, rather than higher-order persistence associated with explosive roots or linear deterministic trends.

Beyond the type of trend, our results seem to undercut the claim that a change in ocean heat exchange in the southern Pacific Ocean has caused a hiatus in warming. Although the mean temperature seems not to rise in both the NH and SH, on-going changes in the variance, skewness, and/or kurtosis do not seem to change. The lack of changes in these higher order moments seems inconsistent with the hypothesis that the stability of the hemispheric means is caused by a change in a deterministic trend.

Similarly, the values of variance, skewness, and/or kurtosis seem inconsistent with the hypothesis that the southern Pacific Ocean increased its uptake of heat in the late 1990's and that this increased heat uptake caused a hiatus in warming. If there were a sudden change in heat uptake, one would expect that there would be a corresponding change in the variance, skewness, or kurtosis of temperature anomalies in the SH relative to the NH. But as indicated in Figures 2-4, no such changes are evident. If the moments do in fact contain such changes – whether due to changes in the direction of stochastic trends in the moments, as we argue, or due to a broken deterministic trend, as others argue for the mean – these changes are more apparent during or before the 1970's.

Finally, the totality of results argues against a ‘runaway greenhouse gas effect.’ According to this hypothesis, rising temperatures trigger a positive feedback loop that increases greenhouse gas concentrations by reducing the solubility of carbon dioxide in seawater (Woolf *et al.*, 2016), changing the balance between respiration and photosynthesis in terrestrial biota (Davidson *et al.*, 2006), and/or releasing methane from methane hydrates (Archer, 2007) and thereby raising temperatures further. Consistent with this possibility, annual variations in the flux of carbon from soils to the atmosphere are positively correlated with mean annual temperature (Raich *et al.*, 2002). Similarly, statistical analyses indicate that increases in global temperature have a small positive effect on atmospheric CO₂ (Keeling *et al.*, 1989; Kaufmann *et al.*, 2006).

Triggering a positive feedback loop would increase the persistence of temperature means. But we find no evidence for such higher levels of persistence. Furthermore, hemispheric differences in persistence are inconsistent with some components of the positive feedback loop. Most of the world’s terrestrial biota is located in the NH, which also holds the greatest reservoir of methane hydrates that could melt in response to higher temperatures. If triggered, such changes would increase the persistence of the NH temperature anomalies relative to those for the SH. But as discussed previously, persistence is more evident in the SH. Such persistence would be consistent with increasing temperatures causing carbon dioxide to flow from seawater to the atmosphere (ocean surface area is greater in the SH), but the increased persistence in the SH is more likely caused by lower sulfur emissions (as described previously).

5 Conclusion

In order to address the important topic of trend detection in the global and hemispheric distributions of temperature anomalies, we introduce a substantial extension of recently proposed tests for unit roots in time series of distributions. Specifically, our testing scheme is two-sided, so that unit roots can be distinguished not only from stationary distributions but also from deterministic or explosive distributions. Our empirical results directly support one unit root process (stochastic trend) in the Southern Hemisphere and two unit root processes in the Northern Hemisphere and the globe, with no higher-order trending behavior in any of the moments of any of these distributions over time.

The absence of higher-order trends is in line with studies that use cointegration methods to relate the global mean temperature to anthropogenic forcings. Our statistical results do not suggest a runaway greenhouse gas effect over the span of our data. However, we acknowledge the statistical difficulty in distinguishing between a stochastic trend and a deterministic trend with breaks.

The difference that we detect between the number of stochastic trends in the hemispheres suggests an interesting footprint of human activity. Warming due to the emission of greenhouse gases in the NH is countervailed by cooling due to sulfur emissions. We believe that differences in the effects of these types of emissions may drive the distinct stochastic trends detected north of the Equator, where most of world's economic activity occurs. Because the residence time in the atmosphere of the former are much longer than that of the latter, the SH is substantively affected only by warming from greenhouse gases, with no countervailing effect from sulfur emissions.

Further, our distributional approach to trend detection provides a new statistical tool to analyze the persistence in higher-order moments of the time series of global and hemispheric distributions. We find what might be described as global compression in the variance. Specifically, the cross-sectional distributions of temperatures over time appear to be shrinking persistently around the increasing mean. In other words, not only is the global mean increasing, but temperature anomalies appear to be less spread out around the mean anomaly over time.

Looking at stochastically trending behavior in the moments beyond the mean and variance provides some intuition about outlying temperature anomalies, albeit with the qualification that our estimation requires that we omit the most extreme outliers. The distributions show leptokurtic trends – that is, they have become more peaked over time (also consistent with the shrinking variance), while outliers have become more common. Since the distributions are estimated on the same support over time, more outliers mean that

existing anomalies are more likely observed, but these temperatures may be new extremes to some localities, creating records highs or lows. Coupled with the increasing kurtosis, an evidently decreasing skewness in the SH suggests that record highs will continue to be more common than record lows.

Our results suggest a useful and natural extension from detection to attribution of the stochastic components in the temperature anomaly distributions. Because greenhouse gases are well mixed, the global distribution of these gases may be expected to be much more uniform than that of temperature anomalies that we have studied in the paper. Examining the higher-order moments of those distributions may not be nearly as informative, and relating stochastic trends in those moments (if any) to those we have examined in this paper does not seem straightforward. We leave these questions for future research.

References

- Archer, D., 2007, Methane hydrate stability and anthropogenic climate change. *Biogeosciences* 4, 521-544.
- Baillie, R.T. and S.-K. Chung, 2002, Modeling and forecasting from trend-stationary long memory models with applications to climatology. *International Journal of Forecasting* 18, 215-226.
- Ballester, J., F. Giorgi, and X. Rodó, 2010, Changes in European temperature extremes can be predicted from changes in PDF central statistics. *Climatic Change* 98, 277-284.
- Beniston, M., 2015, Ratios of record high to record low temperatures in Europe exhibit sharp increases since 2000 despite a slowdown in the rise of mean temperature. *Climatic Change* 129, 225-237.
- Bloomfield, P., 1992, Trends in global temperature. *Climatic Change* 21, 1-16.
- Bloomfield, P. and D. Nychka, 1992, Climate spectra and detecting climate change. *Climatic Change* 21, 275-287.
- Bosq, D., 2000, Linear processes in function spaces, in: *Lecture notes in statistics*, Vol. 149. Springer, New York.
- Brock, W.A., G. Engström, D. Grass, and A. Xepapadeas, 2013, Energy balance climate models and general equilibrium optimal mitigation policies. *Journal of Economic Dynamics & Control* 37, 2371-2396.

- Brohan, P., J.J. Kennedy, I. Harris, S.F.B. Tett, and P.D. Jones, 2006, Uncertainty estimates in regional and global observed temperature changes: a new dataset from 1850. *Journal of Geophysical Research: Atmospheres* 111, D12106.
- Cahill, N., S. Rahmstorf, and A.C. Parnell, 2015, Change points of global temperature. *Environmental Research Letters* 10, 084002.
- Castruccio, S. and M.L. Stein, 2013, Global space-time models for climate ensembles. *The Annals of Applied Statistics* 7, 1593-1611.
- Castruccio, S., D.J. McInerney, M.L. Stein, F.L. Crouch, R.L. Jacob, and E.J. Moyer, 2014, Statistical emulation of climate model projections based on precomputed GCM runs. *Journal of Climate* 27, 1829-1844.
- Chang, Y., C.S. Kim, and J.Y. Park, 2016, Nonstationarity in time series of state densities. *Journal of Econometrics* 192, 152-167.
- Christiano, L.J., 1992, Searching for a break in GNP. *Journal of Business & Economic Statistics* 10, 237-250.
- Davidson, E.A., and I.A. Janssens, 2006, Temperature sensitivity of soil carbon decomposition and feedbacks to climate change. *Nature* 440, 165-173.
- Dergiades, T., R.K. Kaufmann, and T. Panagiotidis, 2016, Long-run changes in radiative forcing and surface temperature: the effect of human activity over the last five centuries. *Journal of Environmental Economics and Management* 76, 67-85.
- Donat, M.G. and L.V. Alexander, 2012, The shifting probability distribution of global daytime and night-time temperatures. *Geophysical Research Letters* 39, L14707.
- Easterling, D. R. and M.F. Wehner, 2009, Is the climate warming or cooling? *Geophysical Research Letters* 36, L08706.
- Estrada, F., C. Gay, and A. Sánchez, 2010, A reply to “Does temperature contain a stochastic trend? Evaluating conflicting statistical results” by R. K. Kaufmann et al. *Climatic Change* 101, 407-414.
- Estrada, F. and P. Perron, 2012, Breaks, trends and the attribution of climate change: a time-series analysis. Department of Economics, Boston University, mimeo.
- Estrada, F. and P. Perron, 2014, Detection and attribution of climate change through econometric methods. *Boletín de la Sociedad Matemática Mexicana* 20, 107-136.

- Estrada, F., P. Perron, C. Gay-García, and B. Martínez-López, 2013, A time-series analysis of the 20th century climate simulations produced for the IPCC's fourth assessment report. *PLoS ONE* 8, e60017.
- Fomby, T.B. and T.J. Vogelsang, 2002, The application of size-robust trend statistics to global-warming temperature series. *Journal of Climate* 15, 117-123.
- Gao, J. and K. Hawthorne, 2006, Semiparametric estimation and testing of the trend of temperature series. *The Econometrics Journal* 9, 332-355.
- Gay-Garcia, C., F. Estrada, and A. Sánchez, 2009, Global and hemispheric temperatures revisited. *Climatic Change* 94, 333-349.
- Gordon, A.H., 1991, Global warming as a manifestation of a random walk. *Journal of Climate* 4, 589-597.
- Gordon, A.H., J.A.T. Bye, and R.A.D. Byron-Scott, 1996, Is global warming climate change? *Nature* 380, 478.
- Hansen, J., R. Ruedy, M. Sato, and K. Lo, 2010, Global surface temperature change. *Reviews of Geophysics* 48, RG000354.
- Hendry, D. and K. Juselius, 2000, Explaining cointegration analysis: Part 1. *Energy Journal* 21, 1-24.
- Johansen, S., 1995, Likelihood-based inference in cointegrated vector autoregressive models. Oxford University Press, Oxford.
- Jun, M. and M.L. Stein, 2008, Nonstationary covariance models for global data. *The Annals of Applied Statistics* 2, 1271-1289.
- Kärner, O., 1996, Global temperature deviations as a random walk. *Journal of Climate* 9, 656-658.
- Kaufmann, R.K., H. Kauppi, M.L. Mann, and J.H. Stock, 2011, Reconciling anthropogenic climate change with observed temperature 1998-2008. *Proceedings of the National Academy of Sciences* 108, 11790-11793.
- Kaufmann, R.K., H. Kauppi, M.L. Mann, and J.H. Stock, 2013, Does temperature contain a stochastic trend: linking statistical results to physical mechanisms. *Climatic Change* 118, 729-743.

- Kaufmann, R.K., H. Kauppi, and J.H. Stock, 2006a, Emissions, concentrations and temperature: a time series analysis. *Climatic Change* 77, 249-278.
- Kaufmann, R.K., H. Kauppi, and J.H. Stock, 2006b, The relationship between radiative forcing and temperature: what do statistical analyses of the instrumental temperature record measure? *Climatic Change* 77, 279-289.
- Kaufmann, R.K., H. Kauppi, and J.H. Stock, 2010, Does temperature contain a stochastic trend? Evaluating conflicting statistical results. *Climatic Change* 101, 395-405.
- Kaufmann, R.K. and D.I. Stern, 2002, Cointegration analysis of hemispheric temperature relations. *Journal of Geophysical Research* 107, ACL 8-1-ACL 8-10.
- Keeling, C.D., R.B. Bacastow, A.F. Carter, S.C. Piper, T.P. Whorf, M. Heimann, W.G. Mook, and H. Roeloffzen, 1989, A three-dimensional model of atmospheric CO₂ transport based on observed winds: 1. Analysis of observational data, in: D.H. Peterson, (Ed.), *Aspects of climate variability in the Pacific and western Americas*, pp. 165-236.
- Kosaka Y. and S.P. Xie, 2013, Recent global-warming hiatus tied to equatorial Pacific surface cooling. *Nature* 501, 403-407.
- Leeds, W.B., E.J. Moyer, and M.L. Stein, 2015, Simulation of future climate under changing temporal covariance structures. *Advances in Statistical Climatology, Meteorology and Oceanography* 1, 1-14.
- Lewis, S.C. and A.D. King, 2015, Dramatically increased rate of observed hot record breaking in recent Australian temperatures. *Geophysical Research Letters* 42, 7776-7784.
- Magnus, J.R., B. Melenberg, and C. Muris, 2011, Global warming and dimming, the statistical evidence. *Journal of the American Statistical Association*, 106, 452-468.
- McKittrick, R. and T.J. Vogelsang, 2014, HAC-robust trend comparisons among climate series with possible level shifts. *Environmetrics* 25, 528-547.
- Mills, T.C., 2009, How robust is the long-run relationship between temperature and radiative forcing? *Climatic Change* 94, 351-361.
- Myhre, G., D. Shindell, F.-M. Bréon, W. Collins, J. Fuglestvedt, J. Huang, D. Koch, J.-F. Lamarque, D. Lee, B. Mendoza, T. Nakajima, A. Robock, G. Stephens, T. Takemura, and H. Zhang, 2013, Anthropogenic and natural radiative forcing, in: T.F. Stocker,

- D. Qin, G.-K. Plattner, M. Tignor, S.K. Allen, J. Boschung, A. Nauels, Y. Xia, V. Bex, and P.M. Midgley, (Eds.), Climate change 2013: the physical science basis. Contribution of Working Group I to the fifth assessment report of the Intergovernmental Panel on Climate Change. Cambridge University Press, Cambridge, pp. 659-740.
- Park, J.Y. and J. Qian, 2012, Functional regression of continuous state distributions. *Journal of Econometrics* 167, 397-412.
- Pretis, F., M. Mann, and R.K. Kaufmann, 2015, Testing competing models of the temperature hiatus: assessing the effects of conditioning variables and temporal uncertainties through sample-wide break detection. *Climatic Change* 131, 705-718.
- Raich, J.W., C.S. Potter, and D. Bhagawati, 2002, Interannual variability in global soil respiration, 1980-94. *Global Change Biology* 8, 800-812.
- Rajaratnam, B., J. Romano, M. Tsiang, and N.S. Diffenbaugh, 2015, Debunking the climate hiatus. *Climatic Change* 133, 129-140.
- Ramaswamy, V., O. Boucher, J. Haigh, D. Hauglustaine, J. Haywood, G. Myhre, T. Nakajima, G.Y. Shi, and S. Solomon, 2001, Radiative forcing of climate change, in: J.T. Houghton, Y. Ding, D.J. Griggs, M. Noguer, P.J. van der Linden, X. Dai, K. Maskell, and C.A. Johnson, (Eds.), Climate Change 2001: the scientific basis. Contribution of Working Group I to the third assessment report of the Intergovernmental Panel on Climate Change. Cambridge University Press, Cambridge, pp. 349-416.
- Shine K.P., R.G. Derwent, D.J. Wuebbles, and J.-J. Morcrette, 1991, Radiative forcing of climate, in: J.T. Houghton, G.J. Jenkins, and J.J. Ephramus, (Eds.), Climate change: the IPCC scientific assessment. Report prepared for Intergovernmental Panel on Climate Change by Working Group I. Cambridge University Press, Cambridge, pp. 41-68.
- Stern, D.I. and R.K. Kaufmann, 2000, Is there a global warming signal in hemispheric temperature series: a structural time series approach. *Climatic Change* 47, 411-438.
- Wergin, G. and J. Krug, 2010, Record breaking temperatures reveal a warming climate. *Europhysics Letters* 92, 30008.
- Woodward, W.A. and H.L. Gray, 1993, Global warming and the problem of testing for trend in time series data. *Journal of Climate* 6, 953-962.

- Woodward, W.A. and H.L. Gray, 1995, Selecting a model for detecting the presence of a trend. *Journal of Climate* 8, 1929-1937.
- Woolf, D.K., P.E. Land, J.D. Shutler, L.M. Goddijn-Murphy, and C.J. Donlon, 2016, On the calculation of air-sea fluxes of CO₂ in the presence of temperature and salinity gradients. *Journal of Geophysical Research: Oceans* 121, 1229-1248.
- Zheng, X. and R.E. Basher, 1999, Structural time series models and trend detection in global and regional temperature series. *Journal of Climate* 12, 2347-2358.
- Zheng, X., R.E. Basher, and C.S. Thompson, 1997, Trend detection in regional-mean temperature series: maximum, minimum, mean, diurnal range, and SST. *Journal of Climate* 10, 317-326.